



HAL
open science

Identifying simultaneously hyper-viscoelastic parameters from a unique heterogenous relaxation test: application to engineering elastomeric materials

Adel Tayeb, Noelie Di Cesare, Yaodong LU, Leonardo Sales, Guilherme Bastos, Jean-Benoit Le Cam

► To cite this version:

Adel Tayeb, Noelie Di Cesare, Yaodong LU, Leonardo Sales, Guilherme Bastos, et al.. Identifying simultaneously hyper-viscoelastic parameters from a unique heterogenous relaxation test: application to engineering elastomeric materials. *Meccanica*, 2023, 58, pp.1983-2002. 10.1007/s11012-023-01706-w . hal-04225728

HAL Id: hal-04225728

<https://hal.science/hal-04225728>

Submitted on 11 Dec 2023

HAL is a multi-disciplinary open access archive for the deposit and dissemination of scientific research documents, whether they are published or not. The documents may come from teaching and research institutions in France or abroad, or from public or private research centers.

L'archive ouverte pluridisciplinaire **HAL**, est destinée au dépôt et à la diffusion de documents scientifiques de niveau recherche, publiés ou non, émanant des établissements d'enseignement et de recherche français ou étrangers, des laboratoires publics ou privés.

052 properties are acquired by adding fillers to the
053 rubber compound, typically carbon black aggre-
054 gates, silica or both. Fillers have a significant effect
055 on the main phenomena involved in mechanical
056 behavior: viscoelasticity [1], the Mullins effect
057 [2, 3], the Payne (or Fletcher-Gent) effect [4, 5],
058 cavitation [6–8], the onset of stress-induced crys-
059 tallization and the crystallinity level [9–13], and
060 possible couplings between them. Concerning the
061 modeling of the mechanical behavior of rubbers
062 and more generally soft materials, the framework
063 of hyperelasticity is often chosen, for instance for
064 tissues [14–16], laminates [17, 18] and specimens
065 [19]. Hyperelastic models are classically identified
066 from several homogeneous tests, see [20] and [21]
067 for instance, since the values of their constitutive
068 parameters generally depend on the strain state
069 [22]. Three homogeneous tests are usually consid-
070 ered, namely the uniaxial tension (UT), the pure
071 shear (PS) and the equibiaxial tension (EQT), to
072 completely describe the domain of possible load-
073 ing paths [23–26]. A trade-off between the sets
074 of values obtained with these different tests has
075 therefore to be found to obtain parameters that
076 can reasonably be considered as intrinsic to the
077 mechanical behavior of the material. As explained
078 in [26] and [27], such identification approach
079 exhibits many disadvantages, among them (i) sev-
080 eral sample geometries (*i.e.* molds) and testing
081 devices are required, (ii) the elaboration process
082 can differ from one sample geometry to another
083 one (typically compression molding versus injec-
084 tion molding), and (iii) the equivalence of max-
085 imum stretch to apply for the different tests is
086 a debated issue when identifying the stabilized
087 behavior. This has a significant effect on the val-
088 ues of the identified constitutive parameters and
089 therefore on the predicted mechanical response
090 [28]. Moreover, the time needed to proceed the test
091 and to process the data is significant for identifi-
092 ing the constitutive parameters for one material.
093 An alternative methodology consists in perform-
094 ing only one heterogeneous test by stretching a
095 3-branch [29] or a 4-branch (cruciform) [26, 30–32]
096 specimen. Such type of test induces a wide range
097 of very different stress/strain states in the sample
098 (typically from UT to EQT). The identification of
099 constitutive parameters is performed by using the
100 measured force(s), generally accompanied by mea-
101 sured kinematic fields [26, 29, 33, 34].

102 Another phenomenon strongly influences the

mechanical behavior; the time dependency of the
stress, which is generally assumed to be due to
viscosity [1, 35–38], even though this assump-
tion should not be applied systematically (see
for instance the discussion in [39]). Viscous (or
time-dependent) effects are classically character-
ized by using two types of additional tests, typi-
cally relaxation and creep tests, which are carried
out under homogeneous loadings, typically ten-
sion/compression. This increases significantly the
characterization time and the number of sam-
ples to be tested. One study proposed to identify
hyper-viscoelastic parameters from several uniax-
ial compression tests [40]. The authors used the
Mooney model [41] and a viscoelastic part based
on the generalized Maxwell model. Nevertheless,
the effect of multiaxiality was not investigated
in this study and several tests were required. It
should be noted that, in this study, the iden-
tification is performed with the Particle Swarm
Optimization (PSO) approach. This optimization
algorithm is well suitable for solving minimization
problems with a wide range of parameters [42–
47], which is typically the case of some elastomeric
materials exhibiting very complex behaviors, with
non-linear elasticity, time-dependency, permanent
set, stress softening, anisotropy, strain-induced
crystallization, to name a few (see for instance
[48]).

In this paper, we investigate to what extent
only one single heterogeneous relaxation test car-
ried out with a 4-branch specimen could be suffi-
cient to identify the hyper-viscoelastic constitutive
parameters of a model describing the behavior of
an engineering elastomeric material by using an
artificially smart population-based metaheuristic
optimization process. The minimization problem
is solved by using the Inverse-PageRank-Particle
Swarm Optimization (I-PR-PSO) algorithm [49].
In addition, in order to allow the widest possible
dissemination of the methodology, we also investi-
gate whether measuring the force only along one
direction of the cruciform specimen could be suffi-
cient for identification, *i.e.* without using full kine-
matic field measurements to build the objective
function. For that purpose, a sensitivity analy-
sis has been carried out in order to evaluate the
values of the displacement and displacement rate
that maximize the identifiability of all constitu-
tive parameters, that is maximizing the sensitivity
of the objective function to the considered design

variables. Also, the analysis investigates the sensitivity to the amount of experimental data (number of force values) used as input data in the objective function calculation.

In Section 2, the sensitivity analysis is presented and the results highlight the loading conditions to be prescribed to maximise the constitutive parameters identifiability. Then, the identification procedure based on the I-PR-PSO algorithm is presented. A numerical validation of the methodology is performed.

In Section 3, the loading conditions previously defined by the sensitivity analysis are applied to a cruciform specimen, to identify the constitutive parameters describing the behavior of its constitutive material. Then, an experimental test with a different loading from the one used for the identification is performed, to fully validate that the material's behavior is well predicted in different loading conditions. The experimental setup is presented, as well as metrology considerations and hardware specifications. In Section 4, the results are presented. The constitutive parameters are identified from the measured force versus time curve, the corresponding constitutive parameters are identified, and the results, in terms of errors between effective and identified behaviors, are presented and discussed. Concluding remarks close the paper.

2 A sensitivity analysis to define the optimal boundary conditions of the test

The aim of this part is to determine, by using a sensitivity analysis procedure, the optimal boundary conditions maximizing the identifiability of the constitutive parameters of the considered hyper-visco elastic model. The identifiability is defined as the sensitivity of the objective function to the design variables (here, the constitutive parameters to be retrieved). *In fine*, the aim is to define the displacement and displacement rate to be prescribed during the experimental test to ensure the best identifiability of the constitutive parameters. Moreover, the minimum experimental data to be used within the identification process for a successful identification has been investigated.

2.1 Definition of the Finite Element (FE) model

The problem to be solved is the identification of the hyper-viscoelastic behavior of an elastomeric material. The geometry chosen is a four-branch 105 mm long and 2 mm thick cruciform specimen, as presented in Fig. 1. It should be noted that this type of multibranch geometry has been increasingly used in the literature [26, 29–32]. The FE model is developed within the ANSYS APDL environment [50], by considering plane stress state and material incompressibility. The four-noded PLANE182 element is used for the calculation. The mesh is made of 9600 nodes and 9363 elements. The mechanical test consists in two phases; the first one is an equibiaxial tensile loading phase, denoted EQT in the following, the second one is a relaxation phase keeping constant the maximum grips displacement, denoted REL in the following.

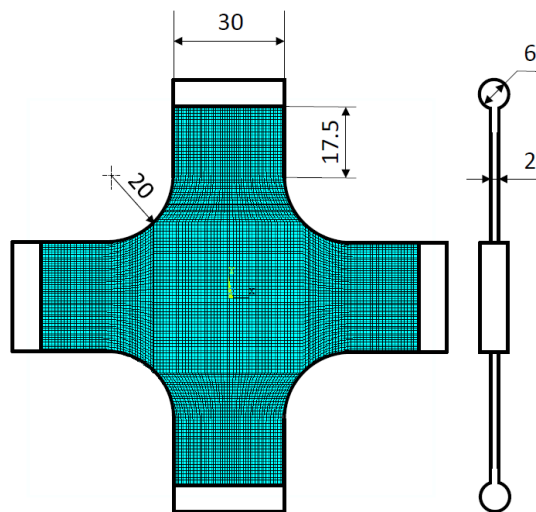


Fig. 1 Geometry of the cruciform specimen. Dimensions in mm.

The hyper-viscoelastic model implemented in ANSYS software is the one due to the Simo model [51]. Assuming pure elastic response in bulk and incompressibility, the constitutive equation for the Cauchy stress tensor is given as in following Eq. (1), where $dev(\bullet) = (\bullet) - \frac{1}{3}[\mathbf{I} : (\bullet)]\mathbf{I}$ denotes the deviator operator in the current configuration, $\mathbf{F}_t(t')$ is the relative deformation gradient tensor at time t' with respect to the configuration at time t , $g(t)$ is the normalized shear relaxation function

$$\boldsymbol{\sigma} = \boldsymbol{\sigma}_o^d + dev \int_0^t \frac{\partial g(t')}{\partial t'} (\mathbf{F}_t^{-1} (t - t') \boldsymbol{\sigma}_o^d (t - t') \mathbf{F}_t^{-t} (t - t')) dt' + p\mathbf{I}, \quad (1)$$

$$\begin{aligned} \boldsymbol{\sigma}_o &= 2\mathbf{B} \frac{\partial \Psi_Y(\mathbf{B})}{\partial \mathbf{B}} \\ W_Y &= C_{10}(I_1 - 3) + C_{20}(I_1 - 3)^2 + C_{30}(I_1 - 3)^3. \end{aligned} \quad (2)$$

and p is an undetermined pressure due to incompressibility. For sake of clarity, long equations will be spanned over the page and displayed within the next few pages. $\boldsymbol{\sigma}_o^d = dev(\boldsymbol{\sigma}_o)$ is the deviatoric part of the instantaneous elastic Cauchy stress tensor $\boldsymbol{\sigma}_o$ derived from the Yeoh [52] instantaneous stored elastic energy density, which is expressed in terms of the first invariant of the left Cauchy-Green tensor \mathbf{B} as given in following Eq. (2).

The three constitutive parameters for the hyperelastic part of the model to be identified within the identification process are C_{10} , C_{20} and C_{30} . The normalized shear relaxation function is expressed as a Prony serie, a sum of decaying exponential functions, as follows

$$g(t) = g_\infty + \sum_i^3 A_i \exp(-\frac{t}{T_i}). \quad (3)$$

The parameters to be identified through the identification process for the viscoelastic part of the model are the three time constants T_1 , T_2 and T_3 and their corresponding relaxation coefficients A_1 , A_2 and A_3 . The long term relaxation coefficient g_∞ is deduced from equation (3) for the starting time ($t = 0$). To be able to determine these constitutive viscoelastic parameters, a creep test can be used as well as a relaxation test.

In an ideal configuration, the initial loading is applied instantaneously. Although, in real life, limitations in the used testing machines limit the loading rate, so the loading time is too long for the results to be used. Then, only the data obtained during the constant displacement or constant load are used to determine the viscoelastic constitutive parameters. In this work, the general Maxwell model implies 3 branches, which implies 6 constitutive parameters to be identified (A_1 , A_2 , A_3 , T_1 , T_2 and T_3 , by varying i from 1 to 3 in Eq. (3)).

The loading rate V [mm/min] and prescribed

displacement D [mm] constituting the boundary conditions of the equibiaxial loading phase of the test are considered as variables to be determined for the identification calculation to be successful.

2.2 Definition of the objective function

The optimization process aims at determining the constitutive parameters for the predicted data to fit the experimental ones. Experimental data considered here are the reaction force at the branches' ends at different displacement levels. The objective function is the sum of two parts, corresponding to the two test phases. The first one is defined to quantify the obtained error during the equibiaxial tensile loading phase of the test, noted EQT in the following. The error is modeled by a squared relative difference between the experimental (exp) and predicted (pred) forces, as follows:

$$E_{EQT} = \sum_{i=1}^n \left(\frac{F_{exp,i} - F_{pred,i}}{F_{exp,i}} \right)^2 \quad (4)$$

where n is the number of points of the EQT force-time curve used to calculate the objective function. n is considered as a variable to be determined, to minimize the data quantity to be stored, while identifying the material's behavior with minimal errors. The second one quantifies the obtained error during the relaxation phase of the test, noted REL in the following. The error is modeled to take the relative curve shape into account without being penalized by the algorithm relative success to retrieve the maximum force value F_{max} (at the beginning of the relaxation phase). The error is then defined as a squared relative difference between the experimental (exp) and

predicted (pred) forces, as follows:

$$E_{REL} = \sum_{j=1}^m \left(\frac{F_{exp,j}}{F_{exp,max}} - \frac{F_{pred,j}}{F_{pred,max}} \right)^2 \quad (5)$$

where m represents the number of points of the REL force-time curve used to process the fitness calculation. m is considered as a variable to be determined.

Finally, the objective function used within the sensitivity analysis and optimization process is given as follows:

$$E_{TOT} = E_{EQT} + E_{REL} \quad (6)$$

The objective function given in Eq. (6) aims at fitting the experimental force-time curve of the whole test (EQT and REL), by determining the constitutive parameters of the chosen constitutive equations. n and m are considered as variables to be determined, to investigate the effect of the sampling on the identifiability of the constitutive parameters to be retrieved.

2.3 Sensitivity analysis

In this section, the optimization variables are the constitutive parameters of the material model, to be identified within the identification process. The sensitivity analysis aims at determining the effect of the optimization variables on the objective function to be minimized, that is its sensitivity, while determining the best boundary conditions of the test (*i.e.* the prescribed displacement D and loading rate V) to be carried out to maximize this sensitivity.

The sensitivity analysis methodology used is based on the Morris method [53], which is a variant of the One-At-a-Time (OAT) method [54]. This method gives indicators (mean and standard deviation (std) of the sensitivity for each parameter) allowing the qualitative classification of the parameters within 3 classes:

- Class #1: those for which the effect on the objective function is negligible (small mean and small std),
- Class #2: those exhibiting a linear effect on the objective function (large mean and small std),
- Class #3: those for which the effect on the objective function is non-linear and/or that

exhibit interactions with other variables (large std).

The methodology is described as follows. First of all, each optimization variable, denoted v_k in the following, is defined on a research domain, which is discretized into 5 sub-domains of size Δv_k . Then, a two-step process is applied:

- Step #1: a first random set of the optimization variables is used in an initial objective function calculation,
- Step #2: the design variables v_k are modified, one-at-a-time, of one step $\pm \Delta v_k$ (the sign is randomly defined) in their respective domain. For each modified variable, the objective function is calculated and the sensitivity s_{v_k} of each of them is determined as the finite difference calculated as in following Eq. (7) where p is the number of optimization variables.

As all variables are modified each time of one step Δv_k in their respective domain - representing 1/5 of the domain - the sensitivity can be normalized, meaning that the denominator can be simplified, so that the sensitivity of each objective function due to the modification of each variable v_k is given as the objective function difference between two consecutive objective function calculations, as given in following Eq. (8).

The whole process (steps #1 and #2) is repeated N times by varying i in Eq. (8), for the results to be statistically representative of the considered research domains. N different values of sensitivity are then obtained, for each considered optimization variable. The mean and standard deviation of these sensitivities are calculated as follows:

$$\mu_{v_k} = \frac{1}{N} \sum_{i=1}^N (S_{v_k})_i \quad (9)$$

$$\Sigma_{v_k} = \sqrt{\frac{1}{N} \sum_{i=1}^N ((S_{v_k})_i - \mu_{v_k})^2} \quad (10)$$

where μ_{v_k} and Σ_{v_k} are the mean and standard deviation of the objective function sensitivity to variable v_k , respectively.

In practice, the optimization variables are discretized in their respective domain as given in Table 1. Here, C_{20} is imposed to be negative for the Yeoh model, in order to fairly predict the shear modulus for all ranges of strain, as

$$s_{v_k} = \frac{OF(v_1, v_2, \dots, v_k \pm \Delta v_k, \dots, v_p) - OF(v_1, \dots, v_p)}{\Delta v_k} \quad (7)$$

$$(S_{v_k})_i = OF_i(v_1, v_2, \dots, v_k \pm \Delta v_k, \dots, v_p) - OF_i(v_1, \dots, v_p) \quad (8)$$

explained in [52]. The stability criterion defined by Drucker [55] is used within the FE code ANSYS APDL in order to ensure the behavior law stability.

Table 1 Discretization of the design variables

Variable	min	max	Step Δv_k
C_{10}	0.1	1	0.18
C_{20}	-0.015	-0.001	0.0028
C_{30}	$1E-4$	$1E-2$	$1.98E-3$
A_1	$1E-4$	0.2	$3.998E-2$
A_2	$1E-4$	0.2	$3.998E-2$
A_3	$1E-4$	0.2	$3.998E-2$
T_1	$1E-4$	1	$1.9998E-1$
T_2	1.0001	10	1.79998
T_3	10.0001	28	3.59998

As the sensitivity analysis aims at determining the best loading conditions to be prescribed during the tests to increase the identifiability of the constitutive parameters, the displacement rate V [mm/min] and prescribed displacement D [mm] are discretized in their respective domains, by taking into account the experimental feasibility of the experimental setup. Thus, the displacement rate V [mm/min] is discretized from 100 to 500 mm/min by step of 100 mm/min . The prescribed displacement D is discretized from 10 to 70 mm , by step of 20 mm . The whole sensitivity process previously described is performed for each set (V ; D).

To validate the methodology, the experimental force-time curve needed to calculate the objective function previously given in Eq. (4) is obtained numerically with the FE calculation previously described. The constitutive parameters of this model are given in Table 2. The value of the incompressibility parameter K^{-1} was set to $10^{-5} MPa^{-1}$ for all the FE calculations proceeded, which is low enough to model the material incompressibility [56]. The number of points obtained from the FE calculation on the force-time curve are, for all the performed calculations: 20 points

evenly distributed during the equibiaxial tension part of the test, 50 points evenly distributed during the first half of the relaxation part of the test, and 20 points evenly distributed during the second half part of the relaxation part of the test.

Finally, the number of points used within the objective function calculation (n and m in Eqs. (4) and (5) respectively) has also been investigated. Then, all these sensitivity calculations are performed by considering five different cases for n and m independently, as follows: 1 point over q are used within the objective function calculation, $\forall q \in [1; 5]$. The global sensitivity calculation algorithm is given in Alg. 1.

2.4 Results of the sensitivity analysis

For each (V ; D) couple, a graphical representation of the influence of each design variable on the objective function is plotted in Fig. 2, representing the results obtained, by prescribing a displacement from 10 to 70 mm , and for a displacement rate from 100 to 500 mm/min (standard deviation (std) as a function of the mean, for each graph). To be able to easily identify the constitutive parameters, their respective sensitivity has to be of the same order of magnitude with respect to each other. This order of magnitude, that is the relative values of sensitivity compared to each others, is the best indicator of the variables' sensitivity, instead of the variables' values themselves (the scale is not of importance in Fig. 2 [53]). Otherwise, the variation of the objective function due to the modification of the less important variables will not be detected as the identification will be going on. As one can see in Fig. 2, for small values of V and D (bottom-left of Fig. 2), C_{10} exhibits a much higher influence on the objective function than the other constitutive parameters. Then, in this case, the other constitutive parameters will not be identifiable by the optimization process, as their influence is small compared to C_{10} influence. On the contrary, with higher values of V and D

Table 2 Constitutive parameters of the numerical model, for its force-time curve to be used as an experimental one in the objective function calculation

Variable	C_{10}	C_{20}	C_{30}	A_1	A_2	A_3	T_1	T_2	T_3
value	0.5	-0.02	0.005	0.09	0.08	0.07	0.2	2	20

Algorithm 1 Sensitivity analysis methodology

```

for each displacement rate  $V$  do
  for each prescribed displacement  $D$  do
    Calculate the reference force-time curve
    for  $N$  times do
      Define an initial random value for each design variable
      Calculate the first initial objective function with equation (6)
      while all the design variables have not been modified do
        Choose a random design variable  $v_k$ 
        Modify  $v_k$  by random  $\pm\Delta v_k$ 
        Calculate the objective function with equation (6)
        Calculate the sensitivity of the objective function with equation (8)
      end while
    end for
    for each design variable  $v_k$  do
      Calculate the sensitivity mean with equation (9)
      Calculate the sensitivity standard deviation with equation (10)
    end for
  end for
end for

```

(top-right of Fig. 2), the influence of all the design variables are of the same order of magnitude, maximizing the chances for the optimization process to detect their influence on the objective function, and then maximizing their identifiability.

The data quantity used within the objective function calculation has been investigated. Five different cases have been studied, by using $1/q$ points on the force-time EQT and REL curves, with $q \in [1; 5]$. Fig. 3 shows the difference of sensitivity by changing the number of points used within the objective function calculation for a given (V ; D) couple, here 500 mm/min and 70 mm , respectively. One can note that the relative sensitivity of all variables, in terms of the distribution of the (standard deviation;mean) plane is not sensitive to the data quantity. Then, the data quantity to be stored and used within the optimization process (variables n and m in Eqs. (4)-(5) respectively) does not need to be too large as no difference in terms of sensitivity distribution is observed. Then, using 17 points (4 for

the EQT phase (variable n in Eq. (4)), 14 for the REL phase (variable m in Eq. (5))) is sufficient for the optimization process to capture the influence of design variables on the objective function.

To sum-up, this sensitivity analysis points out the three main requirements to successfully carry out the identification:

1. The objective function should normalize the maximal value of effort reached at the end of the equibiaxial part of the experimental test, to be specifically taken into account within the fitting process,
2. the boundary conditions to be used within the experimental test should be a displacement and a displacement rate respectively equal to 70 mm and 500 mm/min for the objective function to be sufficiently sensitive to the variables variations,
3. the number of points on the force-time curve can be very few. Here, with a minimum 1:5 sampling (corresponding to 17 data points), we

358
359
360
361
362
363
364
365
366
367
368
369
370
371
372
373
374
375
376
377
378
379
380
381
382
383
384
385
386
387
388
389
390
391
392
393
394
395
396
397
398
399
400
401
402
403
404
405
406
407
408

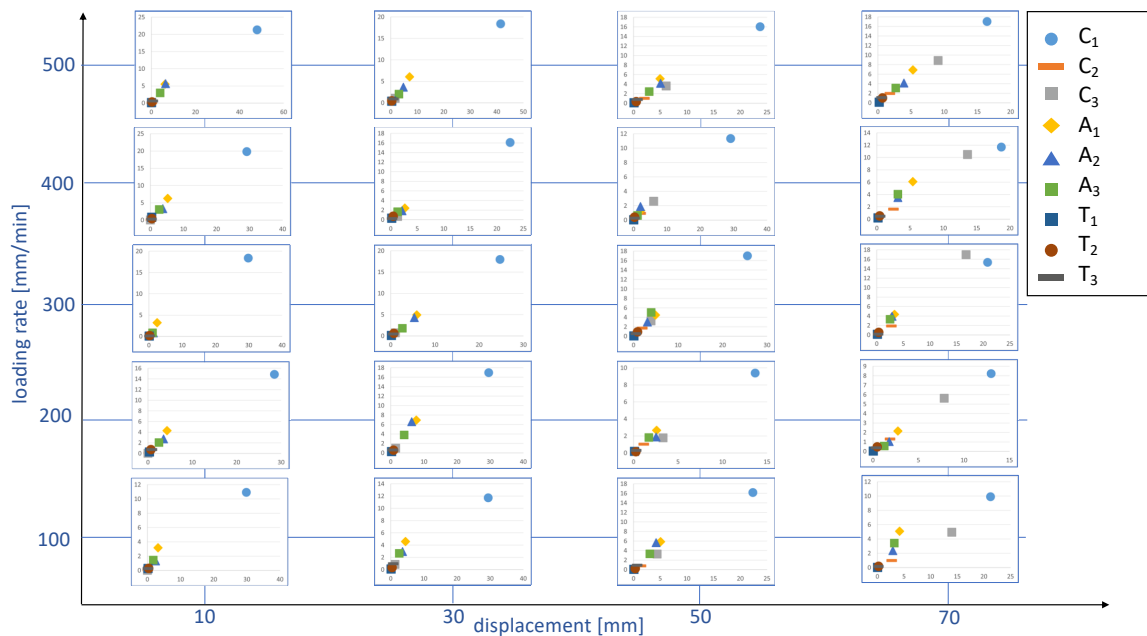


Fig. 2 Evolution of the objective function sensitivity as a function of the loading rate and the prescribed displacement

found the same results as for a 5:5 sampling (corresponding to 90 data points). In practice, this means that it is not necessary to sample the experimental test very precisely, as the number of points does not influence the obtained results, as long as the maximum force reached is measured and identified.

2.5 Identification strategy

Once the experimental boundary conditions have been determined by the sensitivity analysis, a metaheuristic optimization algorithm has been used to identify the constitutive parameters. Inverse-PageRank-PSO (I-PR-PSO) is based both on the Particle Swarm Optimization (PSO) [42, 45, 57] and the PageRank [58, 59] algorithms. By ranking the particles in a smart way, defined by an inverse PageRank strategy [49, 60], this algorithm is strongly decreasing the number of iterations, and so the number of fitness calculation

calls needed to obtain an optimized solution. In I-PR-PSO, as well as in the classical version of PSO, particles are defined, that are each representing a potential solution to the considered objective function. Then, these particles are flying through the research domain, by following each other in a smart way, to converge together to the global optimum of the considered objective function. To do so, the way the particles are influencing each other is considered as a Markov chain. In this way, the probability matrix defining the way the particles are influencing each other, can be deduced from the relative success of each particle at each iteration of the optimization process (for more details, see [49]). Then, the links between particles, is smartly evolving as the calculation is going on, for the best particles to be the most influent upon the swarm. So, at each iteration $k + 1$ of the optimization process, the speed \mathbf{V}_i^{k+1} and position \mathbf{X}_i^{k+1} of every particle i have to be recalculated, by using Eq. (11) where ω is weighing the influence of previous speed on the new one, *i.e.* is representing the inertia of

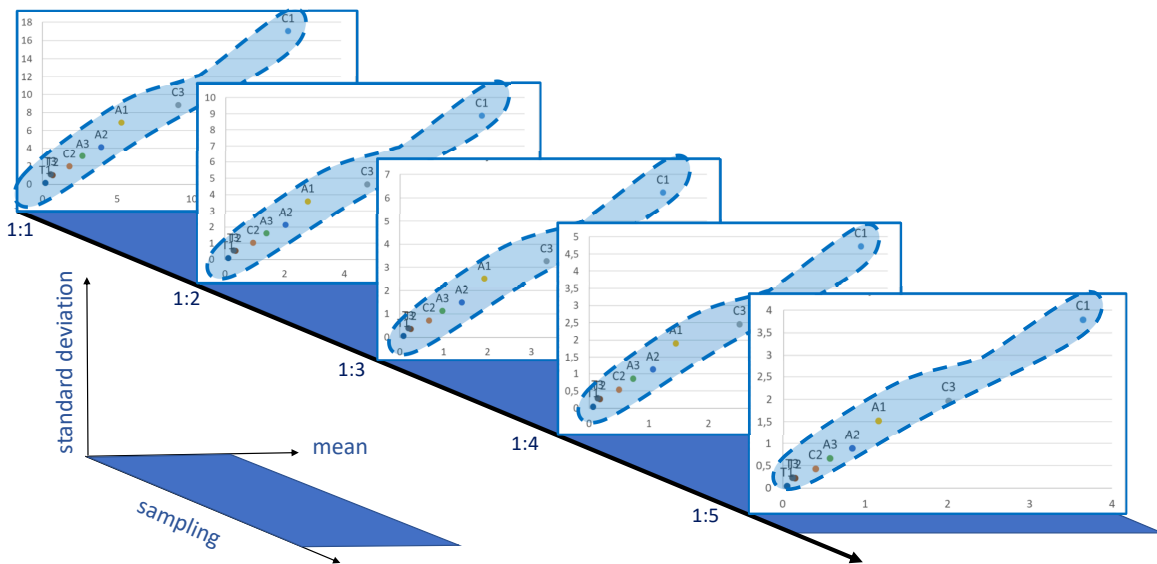


Fig. 3 Evolution of the objective function sensitivity, as a function of the force-time curve sampling

$$\begin{cases} \mathbf{V}_i^{k+1} = \omega \times \mathbf{V}_i^k + rand_1 \times (\mathbf{P}_{i,best}^k - \mathbf{X}_i^k) + rand_2 \times \sum_{j=1}^n C_{ij} \times [\mathbf{P}_{j,best}^k - \mathbf{X}_i^k] \\ \mathbf{X}_i^{k+1} = \mathbf{X}_i^k + \mathbf{V}_i^{k+1} \end{cases} \quad (11)$$

particles during their movement in the research domain, $rand_1$ and $rand_2$ and random numbers in $[0; 1]$ bestowing the heuristic characteristics of the algorithm, $\mathbf{P}_{i,best}^k$ represents the best personal position of particle i found so far. C_{ij} is the probability transition matrix containing the coefficients weighing the influence of all the particles on the others, based on their relative success among the swarm (for more details, see [49]).

In our case, consisting of the identification of the constitutive parameters of an hyper-viscoelastic law, each particle is a vector containing some values of the constitutive parameters that are going to be tested among the fitness calculation.

2.6 Numerical validation

In this section, the proposed identification methodology is applied to the force-time curve obtained from FE simulation of the biaxial experiment with the prescribed displacement and displacement rate identified by the sensitivity analysis. The constitutive parameters for the hyper-viscoelastic model used in this Section, *i.e.* that are to be retrieved by the identification process, are reported in Table 2. Hence, a numerical simulation using these parameters and the previously defined optimal loading conditions is carried out and used as input data to the identification methodology. Its output data is the identified parameters. The ability of the methodology to retrieve the constitutive parameters is then assessed by comparing the force-time curves

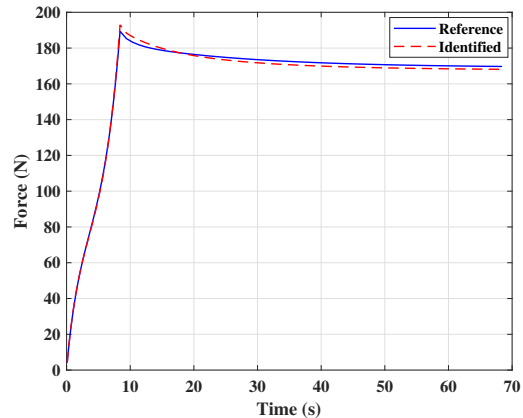
460 obtained with the reference and identified param-
 461 eters as well as the kinematic fields, namely the in-
 462 plane maximum and minimum principal stretches,
 463 by using the same loading conditions.

464 The optimization loop has been launched by con-
 465 sidering the error objective function previously
 466 presented in equation (6).

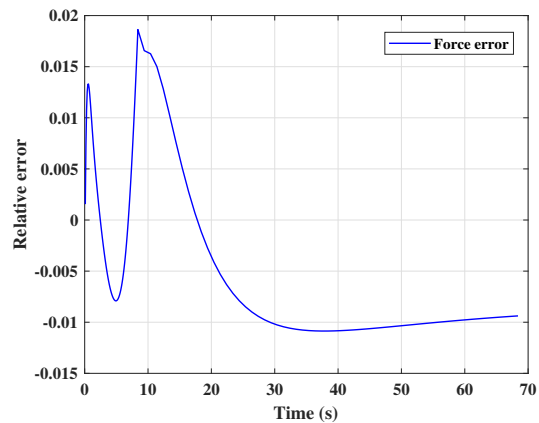
467 The identified parameters are reported in
 468 Table 3. By comparing these values with the con-
 469 stitutive parameters used to launch the theoretical
 470 calculation, previously given in Table 2, one can
 471 see that all the parameters are quite well retrieved,
 472 except for variables T_1 and T_2 for which the error
 473 is superior to 100%. The force-time curves for both
 474 reference and identified parameters and the cor-
 475 responding relative error are reported in Fig. 4.
 476 One can see that the material behavior is well
 477 predicted, even if the variables T_1 and T_2 were
 478 not retrieved. This is explained by the insignif-
 479 icant sensitivity of the objective function to these
 480 two variables (compared to the other ones), as
 481 previously presented in Figs. 2 and 3.

482 In order to validate the identification proce-
 483 dure, an additional biaxial experiment, which was
 484 not used for identifying the constitutive param-
 485 eters, was used. It consists in applying a biaxial
 486 tensile loading with two different displacement
 487 rates following the two directions, followed by a
 488 relaxation of at least 60 s at a displacement of
 489 70 mm. The two displacement rates considered
 490 here were 50 and 500 mm.min⁻¹ in the horizontal
 491 and vertical directions, respectively. The compar-
 492 ison of the kinematic fields at each node of the FE
 493 model is shown in Fig. 5 in terms of the relative
 494 error over the maximum and minimum in-plane
 495 principal stretches.

496 The relative error of the global reaction force
 497 lays between -1.3 % and 1.8 %, which corre-
 498 sponds to an objective function value (Eq. (6)) of
 499 $6.84 \cdot 10^{-3}$. Note that the mean error over the whole
 500 test is under 1 %. On the other hand, from a local
 501 stand point, the relative errors of both kinematic
 502 fields were under 1 % for the maximum displace-
 503 ment applied at the beginning and end of the
 504 relaxation phase. For the maximum in-plane prin-
 505 cipal stretch, this error is maximum for the zones
 506 of equi-biaxial tension, followed by the pure shear
 507 and the uniaxial tension. These errors can differ
 508 of one order of magnitude for these loading cases.
 509 Contrarily, this error is maximum in the zones cor-
 510 responding to a state of pure shear, followed by



(a) Comparison of the reference and identified force-time curves



(b) Relative error of the force

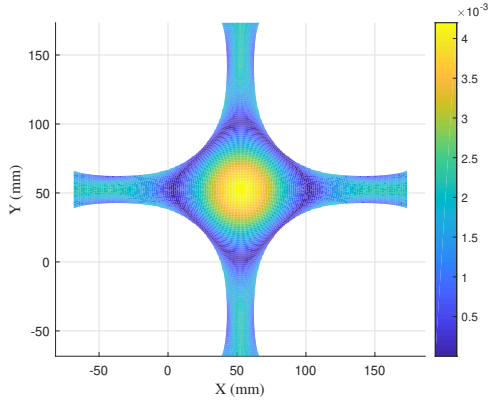
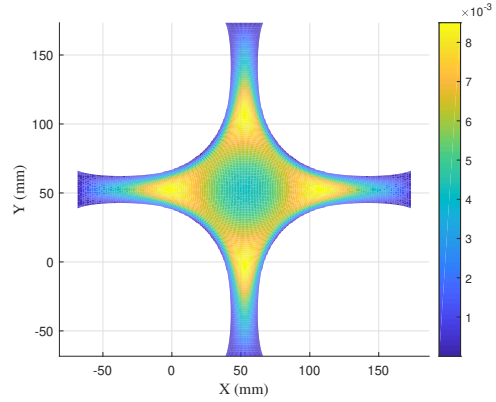
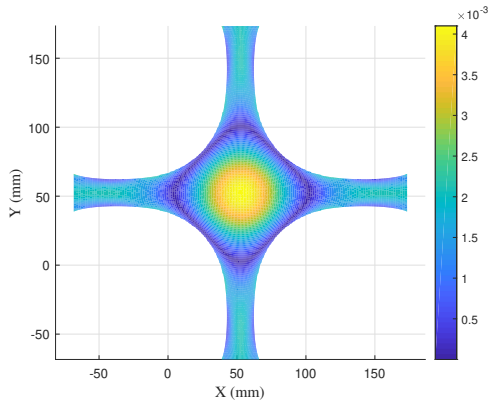
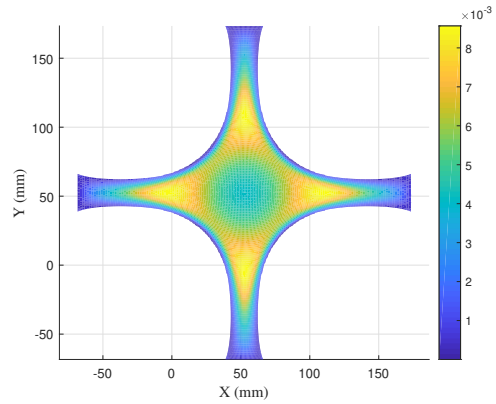
Fig. 4 Comparison of force-time curves between identified and reference parameters

the zones of equi-biaxial tension and uniaxial tension, respectively. Its maximum value is about 8 times its minimum one. These values of the relative errors of both global forces and kinematic fields are very satisfactory.

A significant difference is found between the two in-plane principal stretches λ_{max} and λ_{min} in terms of the relative error. More especially, the field of λ_{min} exhibits a larger relative error in the ring shape zone around the specimen's centre. This is explained by the fact that this zone is under pure shear loading. This is demonstrated by mapping the biaxiality coefficient (this is not presented here because it can be found in recent previous studies [26, 27, 33]), for which the minimum in-plane principal stretch is close to 1, meaning that any variation leads to a significant

Table 3 Identified Constitutive parameters from simulated data

Variable	C_{10}	C_{20}	C_{30}	A_1	A_2	A_3	T_1	T_2	T_3
value	0.496	-0.0246	$5.667 \cdot 10^{-3}$	0.104	0.0767	0.064	0.422	6.434	18.487

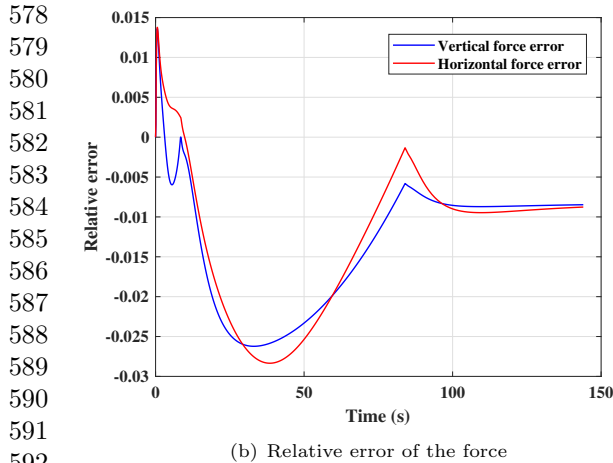
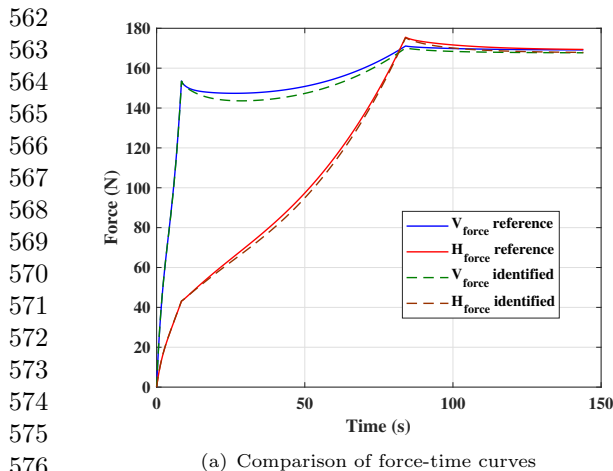
(a) Relative error of λ_{max} at the beginning of relaxation(b) Relative error of λ_{min} at the beginning of relaxation(c) Relative error of λ_{max} at the end of relaxation(d) Relative error of λ_{min} at the end of relaxation**Fig. 5** Relative error of the in-plane maximum and minimum principal stretches obtained from reference and identified parameters

relative error. Moreover, from an experimental point of view, the relative error in this zone will be even more amplified by the measurement noise. This is the reason why the experimental kinematic field of λ_{min} will not be presented in the following.

Furthermore, in order to fully validate the identification procedure, an attempt to predict the mechanical response in terms of the global force and the kinematic fields obtained, with a test that does not serve for the identification, is performed. The test consisted in applying a load up to 70 mm at each branch of the specimen with

two different displacement rates of $500 \text{ mm} \cdot \text{min}^{-1}$ and $50 \text{ mm} \cdot \text{min}^{-1}$ for the vertical and horizontal directions, respectively. The force-time curves for both reference and identified parameters and the corresponding relative error are reported in Fig. 6.

The relative error of the global reaction force varies between -2.9 % and 1.4 %, which is very close to what was obtained for the identification test (between -1.3 % and 1.8 %). The mean error over the whole test is under 1.6 % for the vertical force and 1.5 % for the horizontal one. Moreover, as the material is assumed to be isotropic, at the



593 **Fig. 6** Comparison of force-time curves between identified
594 and reference parameters

596 end of the test, the relaxed horizontal and vertical
597 forces are the same for a given calculation (the
598 reference one or the predicted one). The relative
599 error between the reference and predicted relaxed
600 forces is inferior to 1 %, whatever the direction
601 considered.

602 The results obtained in terms of the relative
603 error in the in-plane principal stretch values at any
604 point of the full-kinematic fields are reported in
605 Fig. 7. The relative error of both kinematic fields
606 were always inferior to 1 %, which is not more
607 than the results obtained during the identifica-
608 tion procedure. This is therefore a very promising
609 result, validating, by the way, the experimental
610 test conditions defined for the identification of the
611 constitutive parameters by the sensitivity analysis
612 previously presented in Section 2. The relative

error fields can be interpreted similarly to the pre-
vious ones, they are therefore not further discussed
in this Section.

In this Section, we have demonstrated, from
the numerical validation of the method, that if
the constitutive model is well adapted to describe
the material's behavior (that is, if its constitu-
tive parameters are well chosen for the predicted
force-time curve to fit the experimental one), the
kinematic fields are well predicted as well even
though they are not used in the objective func-
tion calculation. This confirms the challenging
motivation of the present study, *i.e.* identifying
hyper-viscoelastic parameters from the measured
reaction force only. This is fully addressed in the
next Section.

3 Application to experimental data

In this Section, the identification of the consti-
tutive parameters describing the behavior of a
real-life engineering elastomeric material is first
carried out and validated. Then, another exper-
imental test, not used within the identification
procedure, is proceeded, to fully validate that the
material's behavior is well predicted in different
loading conditions.

3.1 Material and specimen geometry

The material used in this study is a carbon black
filled natural rubber. It has the same dimen-
sion as the one used for the numerical simulation
previously presented in Fig. 1.

3.2 Loading conditions

The experimental set-up is presented in Fig. 8. It
is composed of a home-made biaxial testing machine
and a digital CCD camera. The testing machine
is composed of four independent electrical actu-
ators controlled by an in-house LabVIEW program.
It is equipped with two load cells with a capac-
ity of 1094 N, measuring the force variation in
the two perpendicular directions. In this work, an
equibiaxial load was applied to the cruciform spec-
imen. A displacement of 70 mm was applied to
each branch at a loading rate of 500 mm/min and
the maximum displacement was kept constant for
60 s. It should be noted that the specimen was

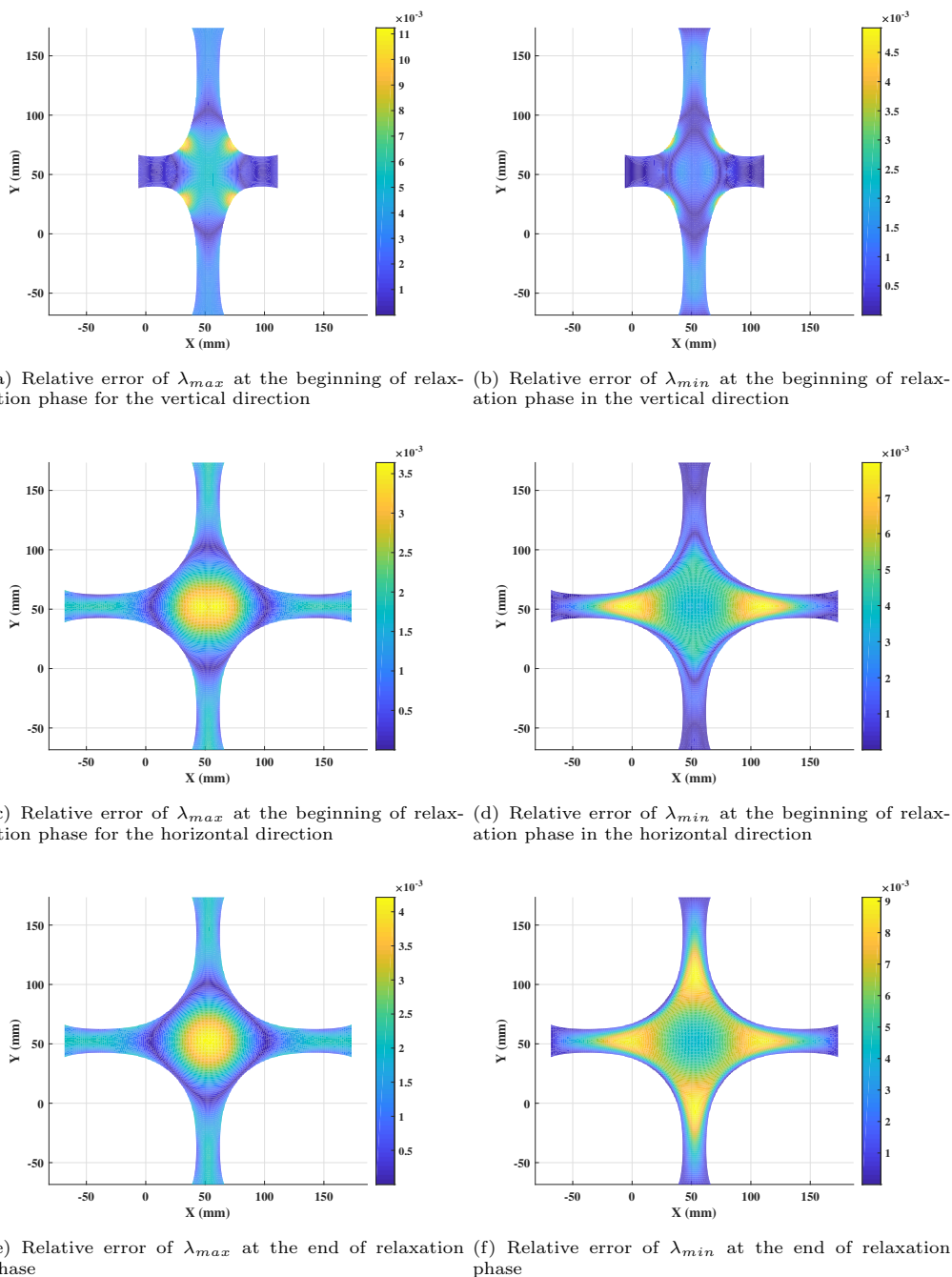


Fig. 7 Relative error of the in-plane maximum and minimum principal stretches obtained from reference and identified parameters

beforehand accommodated by three cycles at the same maximum displacement and a loading rate of 500 mm/min . The maximum applied displacement corresponds to a global stretch λ_{glob} (that is

the ratio between the final and the initial lengths of the specimen in a given direction) of 2.33.

664
665
666
667
668
669
670
671
672
673
674
675
676
677
678
679
680
681
682
683
684
685
686
687
688
689
690
691
692
693
694
695
696
697
698
699
700
701
702
703
704
705
706
707
708
709
710
711
712
713
714

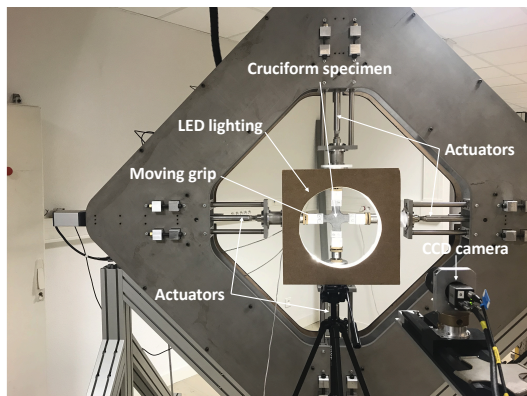


Fig. 8 Overview of the experimental set-up

3.3 Full-field kinematic measurement

Full-field kinematic measurements are used, as well as the measured force, for validating the identification procedure. We recall here that they do not appear in the expression of the objective function because the aim is to propose a method employing as few measurements as possible. Moreover, we have demonstrated in the numerical validation of the method, that if the constitutive model is well adapted to the material behavior, the kinematic fields are well predicted (all the relative errors on the kinematic fields were under 1 %), even if they were not included in the objective function calculation (see Fig. 5). The full-kinematic field at the surface of the stretched specimen was determined by using the Digital Image Correlation (DIC) technique [61]. The correlation process was achieved with the SeptD software [62]. During the experiments, images of the specimen surface were stored at a frequency of 5 Hz using an IDS CCD camera of 1920×1200 joined pixels equipped with a 55 mm telecentric objective. Before the test, the specimen was sprayed by a white paint in order to improve the image contrast and during the test, a home-made LED lighting system appearing in Fig. 8 is used to obtain a uniform cold lighting from the smallest to the highest reached strains. As the test is symmetrical, a rectangular region on one branch of the cruciform specimen is sufficient to apply the identification procedure previously described. The rectangular ROI is represented in Fig. 9. It corresponds to a zone from the sample center to the cylinder at the end of its branch. The gauge block

shown in Fig. 9 is used for converting pixels to millimeters.

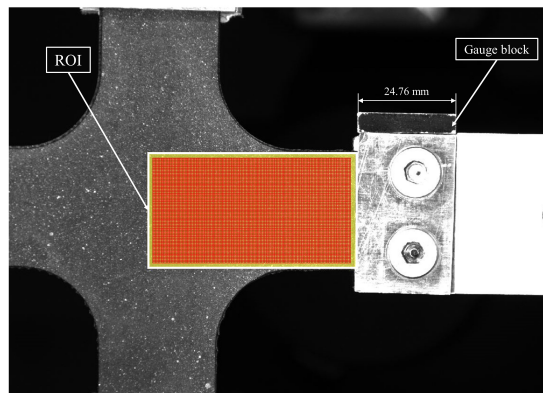


Fig. 9 Region Of Interest (ROI) composed of Zones Of Interest of 30 by 30 pixels ZOIs

Following the recommendation of the DIC guide [63], both DIC hardware and analysis parameters are given in Tables 4 and 5 respectively.

4 Results

The experimental and predicted force-time curves and their corresponding relative errors are reported in Fig. 10.

First of all, the maximum force reached is well predicted (the relative error is inferior to 1 %). Similarly, the curve shape for the relaxation phase is predicted with a maximum relative error inferior to 1.5 %.

The results obtained in terms of the relative error in the in-plane maximum principal stretch values at any point of the full-kinematic fields are reported in Fig. 11.

The maximum relative error obtained was found in the central zone, where the in-plane maximum principal stretch is the lowest, and equates to 12 %. The maximum of the mean error is 5.2 %.

The fact that the maximum relative error obtained for the kinematic field is superior in the experimental study than in the numerical one can be easily explained by several experimental considerations:

Table 4 DIC hardware parameters

Camera	IDS UI-3160CP Rev. 2
Image Resolution	1920 × 1200 pixels ²
Lens	55 mm C-mount partially telecentric. Constant magnification over a range of working distances ± 12.5 mm of object movement before 1 % error image scale occurs
Aperture	f/5.6
Field-of-View	139.4 × 87.1 mm
Image Scale	14 pixels / mm
Stand-off Distance	1100 mm
Image Acquisition Rate	5 Hz
Patterning Technique	White spray on black sample
Pattern Feature Size (Approximation)	6 pixels

Table 5 DIC Analysis parameters

DIC Software	7D [©]
Image Filtering	None
Subset Size	30 pixels / 2.53 mm
Step Size	4 pixels / 0.33 mm
Subset Shape Function	Affine
Matching Criterion	Normalized Cross Correlation
Interpolant	Bi-cubic
Strain Window	5 data points
Virtual Strain Gauge Size	54 pixels / 4.56 mm
Strain Formulation	Logarithmic
Post-Filtering of Strains	None
Displacement Noise-Floor	0.036 pixels / 3.04 μm
Strain Noise-Floor	6.1 mm/m

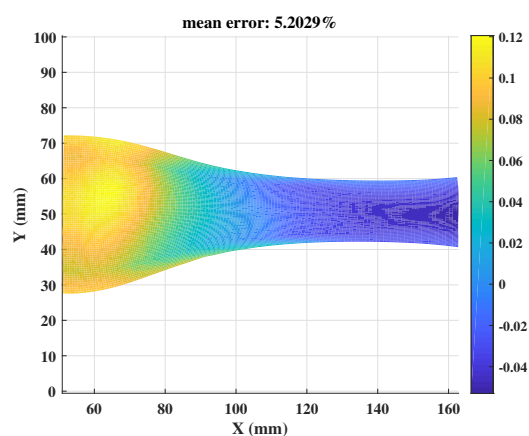
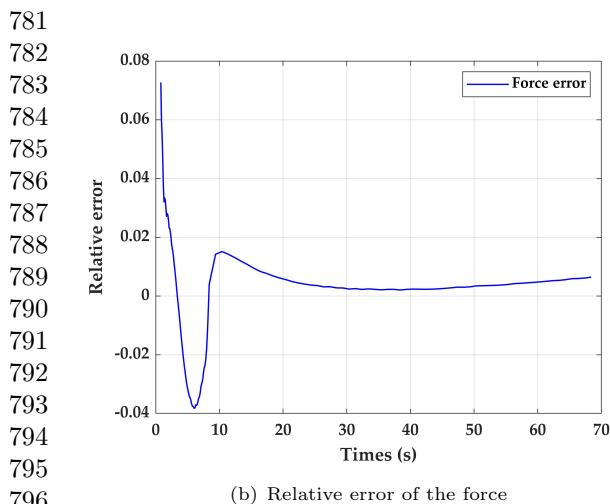
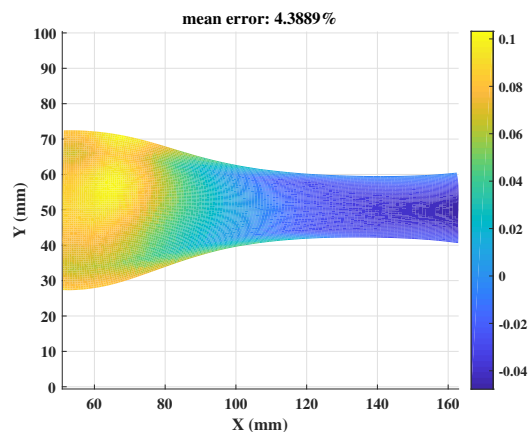
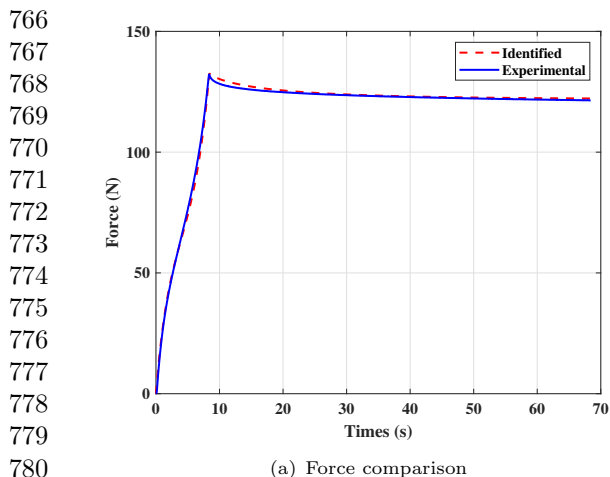
- the noise in the displacement field measurements (it was not evaluated here, as it should not be the main cause of error),
- the positioning of coordinates origin for the experimental fields. It corresponds to the motionless point of the ROI. It is quite challenging to precisely determine its position, as heterogeneities in the material, the accuracy of the displacement measurement and relative spatial resolution of the displacement field compared to the FE grid can make difficult its identification,
- the hyperelastic part of the used model does not perfectly represent the non-linearity of the experimental stress-strain relationship. This is supported by the high value of the relative error

reached during the EQT loading phase (around 7 %).

Regarding the accuracy of the predicted force and full-kinematic fields, the latter being not used for the parameters identification, this is a promising result to validate the proposed identification methodology. This validation will be fully addressed in the next Section.

4.1 Validation

Similarly to the numerical study, the validation is carried out with a new experimental test that was not used for the experimental identification. It is the same as the one used for the numerical validation, *i.e.* a load up to 70 mm at each branch of the



797 **Fig. 10** Comparison of force-time curves between experi-
798 mental and predicted data
799

800 cruciform specimen with two different displace-
801 ment rates of 500 mm.min^{-1} and 50 mm.min^{-1}
802 for the vertical and horizontal directions, respec-
803 tively. Fig. 12 presents the results obtained, in
804 terms of experimental and predicted forces versus
805 time (Fig. 12(a)) and the corresponding relative
806 errors (Fig. 12(b)). The maximum relative error is
807 obtained in the REL phase. It is inferior to 7 %
808 and 9 % for the force in the horizontal and the
809 vertical directions, respectively. These results are
810 very satisfactory considering that the numerical
811 study, for which the measurement noise had not
812 been simulated, led to relative errors lower than
813 3 %.

814 It should be noted that both predicted forces
815 converge towards the same value at the end of the
816

Fig. 11 Relative error of the predicted and measured in-
plane maximum principal stretch plotted in ROI taken in
the horizontal branch

REL phase. This is expected as the constitutive
model is isotropic. This is not the case for the
measured forces, suggesting that non negligible
anisotropic effects occur. Fig. 13 presents the re-
lative error of the measured and predicted in-plane
maximum principal stretches.

5 Conclusion

In this study, a methodology to identify the con-
stitutive parameters of hyper-viscoelastic models
describing the behavior of engineering elastomeric
materials has been proposed. The aim of this
methodology is dual: (i) it is using only one het-
erogeneous test, and (ii) it is minimizing the data
quantity to be stored and processed, by using

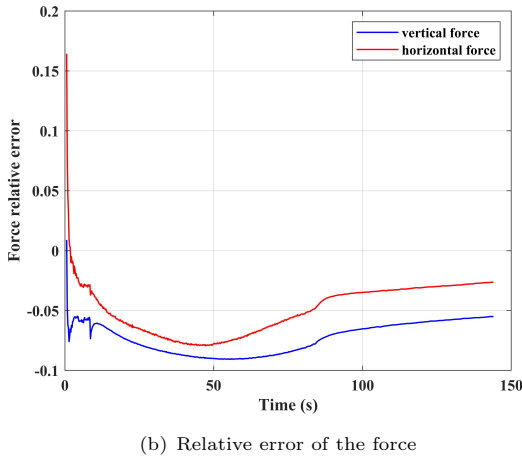
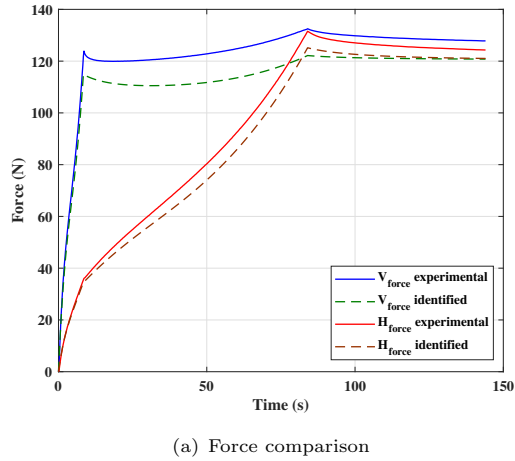


Fig. 12 Comparison of force-time curves between experimental and identified data for the verification test

the reaction force measured during the test only, to determine the solution's quality. To this end, an equibiaxial test is considered, composed of an equibiaxial tension phase, followed by a relaxation phase.

First, an objective function has been defined to efficiently minimize the squared difference between the experimental and predicted force-time curves, during the two phases of the test. This objective function has been calculated by comparing the experimental force-time curves with the one given by a FE analysis. In the FE analysis, the constitutive model is based on the Yeoh model and the Prony series to describe the hyperelastic and viscous behaviors, respectively. These models provide 3 and 6 constitutive parameters

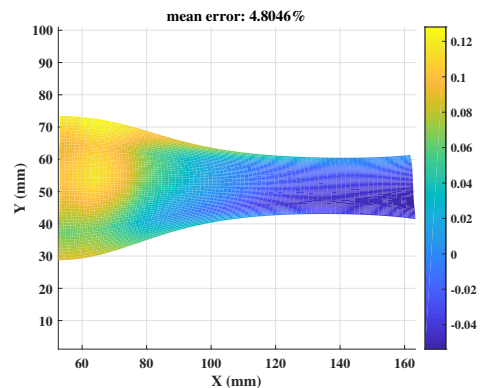
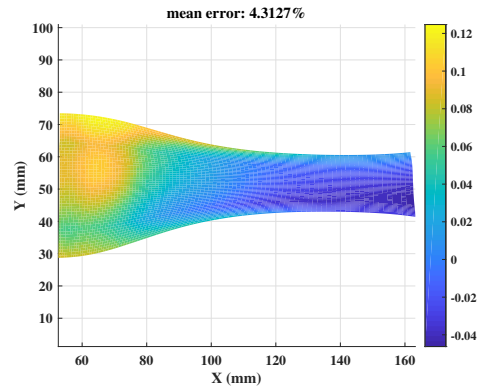
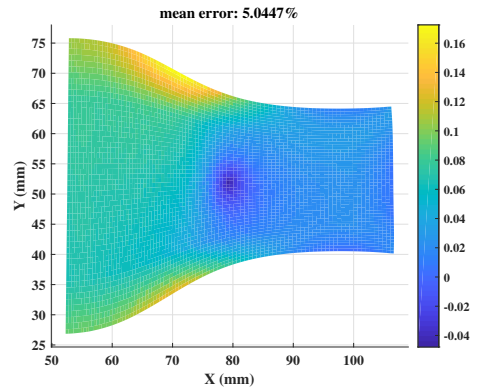


Fig. 13 Relative error of the measured and predicted in-plane maximum principal stretches

868 to be identified within the identification process,
869 respectively.

870 Then, a sensitivity analysis has been devel-
871 oped. This study aims at (i) determining the
872 experimental boundary conditions (displacement
873 rate and prescribed displacement) for the previ-
874 ously defined objective function to be sufficiently
875 sensitive to the considered design variables, and
876 (ii) determining the minimal data quantity (that
877 is the number of points on the force-time curve) to
878 be used for the following identification procedure
879 to be successful.

880 Next, the identification strategy has been
881 developed. It is based on the Inverse-PageRank-
882 PSO algorithm, which is a population-based meta-
883 heuristic optimization method, effectively useful
884 when dealing with minimization problems with
885 a wide range of design variables. This minimiza-
886 tion algorithm is coupled with a FEMU technique,
887 based on the using of the previously presented FE
888 model.

889 Finally, numerical and experimental investi-
890 gations have been performed. In the numerical
891 analysis, the proposed methodology is applied on
892 a case where the experimental data to be fitted is
893 replaced by a numerical one, for which the con-
894 stitutive parameters and the behavior curves are
895 known. The results show small errors on the force-
896 time curves, as well as on the full-kinematic fields
897 (even if they were not used to calculate the objec-
898 tive function during the identification procedure).
899 Another test has been performed, to fully vali-
900 date the fact that the predicted and experimental
901 behaviors were similar, even on a test where the
902 boundary conditions were different from the test
903 used during the identification procedure. Again,
904 this test were successful, validating numerically
905 the proposed methodology by providing very small
906 errors on the force-time curves and on the full-
907 kinematic fields. In the experimental analysis, the
908 force-time curves to be fitted have been obtained
909 experimentally. The proposed methodology was
910 then successful to retrieve the experimental force-
911 time curves, as well as the full-kinematic fields.
912 Again, a new experimental test has been per-
913 formed, in which the boundary conditions are
914 different from the one used during the identifi-
915 cation procedure. The methodology is then fully
916 validated, because the experimental and predicted

917
918

force-time curves and full-kinematic fields were
very close (a few % of error on each of them).

The main interests of the proposed identifica-
tion methodology can be summarized as follows:

- the test duration is reduced,
- only one heterogeneous relaxation test is required,
- only one force measurement, *i.e.* one force cell, is required,
- the use of the PSO in the optimization process is well suitable to identify models with a larger number of parameters, available in FE codes, and by the way to account for phenomena such as accommodation, strain-induced anisotropy, strong non-linearities at large strains, a large number of viscous parameters, non-exhaustively.

Acknowledgments. The authors thank Région Bretagne, Rennes Métropole, Association Française de Mécanique and Université Bretagne Loire for their financial support. The authors also thank Dr Eric Robin, Dr Mathieu Miroir, Mr Vincent Burgaud and Mr Mickaël Le Fur for having designed the biaxial tensile machine.

6 Compliance with Ethical Standards:

The authors declare that they have no conflict of interest.

References

- [1] Tayeb, A., Arfaoui, M., Zine, A., Hamdi, A., Benabdallah, J., Ichchou, M.: On the Non-linear Viscoelastic Behavior of Rubber-like Materials: Constitutive Description and Identification. *International Journal of Mechanical Sciences* **130**, 437–447 (2017). <https://doi.org/10.1016/j.ijmecsci.2017.06.032>
- [2] Mullins, L.: Effect of Stretching on the Properties of Rubber. *Rubber Chemistry and Technology* **21**, 281–300 (1948). <https://doi.org/10.5254/1.3546914>
- [3] Chagnon, G., Verron, E., Gornet, L., Marckmann, G., Charrier, P.: On the relevance of Continuum Damage Mechanics as Applied to the Mullins effect in elastomers. *Journal*

- of the Mechanics and Physics of Solids **52**, 1627–1650 (2004). <https://doi.org/10.1016/j.jmps.2003.12.006>
- [4] Fletcher, W.P., Gent, A.N.: Non-Linearity in the Dynamic Properties of Vulcanised Rubber Compounds. *Trans. Institute Rubber Industry* **29**, 266–280 (1953)
- [5] Payne, A.: The Dynamic Properties of Carbon Black-Loaded Natural Rubber Vulcanizates. Part I. *Journal of Applied Polymer Science* **19**, 53–57 (1962). <https://doi.org/10.1002/app.1962.070061906>
- [6] Stringfellow, R., Abeyaratne, R.: Cavitation in an Elastomer: Comparison of Theory with Experiment. *Materials Science and Engineering: A* **112**, 127–131 (1989). [https://doi.org/10.1016/0921-5093\(89\)90351-1](https://doi.org/10.1016/0921-5093(89)90351-1)
- [7] Le Cam, J.-B., Toussaint, E.: Volume Variation in Stretched Natural Rubber: Competition between Cavitation and Stress-induced Crystallization. *Macromolecules* **41**, 7579–7583 (2008). <https://doi.org/10.1021/ma801290w>
- [8] Le Cam, J.-B., Toussaint, E.: Cyclic Volume Changes in Rubbers. *Mechanics of Materials* **41**, 898–901 (2009). <https://doi.org/10.1016/j.mechmat.2009.02.004>
- [9] Toki, S., Fujimaki, T., Okuyama, M.: Strain-induced Crystallization of Natural Rubber as Detected Real-time by Wide-angle X-ray Diffraction Technique. *Polymer* **41**, 5423–5429 (2000). [https://doi.org/10.1016/S0032-3861\(99\)00724-7](https://doi.org/10.1016/S0032-3861(99)00724-7)
- [10] Toki, S., Sics, I., Ran, S., Liu, L., Hsiao, B.S., Murakami, S., Senoo, K., Kohjiya, S.: New insights into Structural Development in Natural Rubber during Uniaxial Deformation by In Situ Synchrotron X-ray Diffraction. *Macromolecules* **35**, 6578–6584 (2002). <https://doi.org/10.1021/ma0205921>
- [11] Trabelsi, S., Albouy, P.-A., Rault, J.: Stress-induced Crystallization around a Crack tip in Natural Rubber. *Macromolecules* **35**, 10054–10061 (2002). <https://doi.org/10.1021/ma021106c>
- [12] Trabelsi, S., Albouy, P.-A., Rault, J.: Effective Local Deformation in Stretched filled Rubber. *Macromolecules* **36**, 9093–9099 (2003). <https://doi.org/10.1021/ma0303566>
- [13] Huneau, B.: Strain-induced Crystallization of Natural Rubber: a Review of X-ray Diffraction Investigations. *Rubber Chemistry And Technology* **84**(3), 425–452 (2011). <https://doi.org/10.5254/1.3601131>
- [14] Masson, I., Fassot, C., Zidi, M.: Finite Dynamic Deformations of a Hyperelastic, Anisotropic, Incompressible and Prestressed tube. Applications to In vivo Arteries. *European Journal of Mechanics - A/Solids* **29**(4), 523–529 (2010). <https://doi.org/10.1016/j.euromechsol.2010.02.007>
- [15] Chagnon, G., Rebouah, M., Favier, D.: Hyperelastic Energy Densities for Soft Biological Tissues: A Review. *Journal of Elasticity* **120**(4), 129–160 (2015). <https://doi.org/10.1007/s10659-014-9508-z>
- [16] Chaimoon, K., Chindapasirt, P.: An Anisotropic Hyperelastic Model with an Application to Soft Tissues. *European Journal of Mechanics - A/Solids* **78**, 103845 (2019). <https://doi.org/10.1016/j.euromechsol.2019.103845>
- [17] Li, J., Slesarenko, V., Rudykh, S.: Microscopic Instabilities and Elastic Wave Propagation in Finitely Deformed Laminates with Compressible Hyperelastic Phases. *European Journal of Mechanics - A/Solids* **73**, 126–136 (2019). <https://doi.org/10.1016/j.euromechsol.2018.07.004>
- [18] Aguiar, A.R., Perez-Fernandez, L.D., Prado, E.B.T.: Analytical and Numerical Investigation of Failure of Ellipticity for a Class of Hyperelastic Laminates. *European Journal of Mechanics - A/Solids* **61**, 110–121 (2017). <https://doi.org/10.1016/j.euromechsol.2016.09.005>
- [19] Patil, A., DasGupta, A.: Finite Inflation of an Initially Stretched Hyperelastic Circular

- 970 Membrane. *European Journal of Mechanics -*
 971 *A/Solids* **41**, 28–36 (2013). [https://doi.org/](https://doi.org/10.1016/j.euromechsol.2013.02.007)
 972 [10.1016/j.euromechsol.2013.02.007](https://doi.org/10.1016/j.euromechsol.2013.02.007)
- 973
- 974 [20] Bazkiaei, A.K., Shirazi, K.H., Shishesaz,
 975 M.: A Framework for Model Base Hyper-
 976 Elastic Material Simulation. *Journal of Rub-*
 977 *ber Research* **23**(4), 287–299 (2020).
 978 <https://doi.org/10.1007/s42464-020-00057-5>
- 979
- 980 [21] Said, L.B., Wali, M., Khedher, N., Kessentini,
 981 A., Algahtani, A., Dammak, F.: Efficiency of
 982 Rubber-pad Cushion in Bending Process of a
 983 Thin Aluminum Sheet. *Journal of Rubber*
 984 *Research* **23**, 89–99 (2020). [https://doi.org/](https://doi.org/10.1007/s42464-020-00040-0)
 985 [10.1007/s42464-020-00040-0](https://doi.org/10.1007/s42464-020-00040-0)
- 986
- 987 [22] Treloar, L.R.G.: Stress-strain Data for Vul-
 988 canised Rubber under Various Types of
 989 Deformation. *Transactions of the Faraday*
 990 *Society* **40**, 59–70 (1944). [https://doi.org/10.](https://doi.org/10.1039/TF9444000059)
 991 [1039/TF9444000059](https://doi.org/10.1039/TF9444000059)
- 992
- 993 [23] Treloar, L.R.G.: *The Physics of Rubber Elas-*
 994 *ticity*, 3rd edn. Clarendon Press, Oxford
 995 (1975)
- 996
- 997 [24] Ward, I.M., Hadley, D.W.: *An Introduction*
 998 *to the Mechanical Properties of Solid Poly-*
 999 *mers*, 2nd edn. John Wiley and Sons Ltd,
 1000 New-York (1993)
- 1001
- 1002 [25] G'Sell, C., Coupard, A.: *Génie Mécanique des*
 1003 *Caoutchoucs*. ISBN 2-9510704-0-3. Appollor
 1004 et INPL, Ecole des Mines de Nancy (1997)
- 1005
- 1006 [26] Promma, N., Raka, B., Grédiac, M., Tou-
 1007 ssaint, E., Le Cam, J.-B., Balandraud,
 1008 X., Hild, F.: Application of the Virtual
 1009 Fields Method to Mechanical Characteri-
 1010 zation of Elastomeric Materials. *Interna-*
 1011 *tional Journal of Solids and Structures* **46**,
 1012 698–715 (2009). [https://doi.org/10.1016/j.](https://doi.org/10.1016/j.ijsolstr.2008.09.025)
 1013 [ijsolstr.2008.09.025](https://doi.org/10.1016/j.ijsolstr.2008.09.025)
- 1014
- 1015 [27] Charlès, S., Le Cam, J.-B.: Inverse Identi-
 1016 fication from Heat Source Fields: a Local
 1017 Approach Applied to Hyperelasticity. *Strain*
 1018 (2020). <https://doi.org/10.1111/str.12334>
- 1019
- 1020 [28] Marckmann, G., Verron, E.: Comparison of
 Hyperelastic Models for Rubber-like Materi-
 als. *Rubber Chemistry and Technology* **79**,
 835–858 (2006). [https://doi.org/10.5254/1.](https://doi.org/10.5254/1.3547969)
 3547969
- [29] Guélon, T., Toussaint, E., Le Cam, J.-B.,
 Promma, N., Grédiac, M.: A New Character-
 ization Method for Rubbers. *Polymer Testing*
28, 715–723 (2009). [https://doi.org/10.1016/](https://doi.org/10.1016/j.polymertesting.2009.06.001)
[j.polymertesting.2009.06.001](https://doi.org/10.1016/j.polymertesting.2009.06.001)
- [30] Johlitz, M., Diebels, S.: Characterisation of
 a Polymer Using Biaxial Tension Tests. Part
 I: Hyperelasticity. *Arch Appl. Mech.* **81**,
 1333–1349 (2011). [https://doi.org/10.1007/](https://doi.org/10.1007/s00419-010-0480-1)
[s00419-010-0480-1](https://doi.org/10.1007/s00419-010-0480-1)
- [31] Sasso, M., Chiappini, G., Rossi, M.,
 Cortese, L., Mancini, E.: Visco-Hyper-
 Pseudo-Elastic Characterization of a
 Fluoro-Silicone Rubber. *Experimental*
Mechanics **54**(3), 315–328 (2014).
<https://doi.org/10.1007/s11340-013-9807-5>
- [32] Seibert, H., Scheffer, T., Diebels, S.: Biax-ial
 Testing of Elastomers - Experimental Setup,
 Measurement and Experimental Opti-
 misation of Specimen's Shape. *Technische*
Mechanik **81**, 72–89 (2014). [https://doi.org/](https://doi.org/10.24352/UB.OVGU-2017-054)
[10.24352/UB.OVGU-2017-054](https://doi.org/10.24352/UB.OVGU-2017-054)
- [33] Tayeb, A., Le Cam, J.-B., Grédiac, M.,
 Toussaint, E., Balandraud, X.: Identifying
 Hyperelastic Constitutive Parameters with
 Sensitivity-based Virtual Fields. *Strain* **57**
 (2021). <https://doi.org/10.1111/str.12397>
- [34] Bastos, G., Sales, L., Di Cesare, N., Tayeb, A.,
 Le Cam, J.-B.: Inverse-Pagerank-particle
 swarm optimisation for inverse identifica-
 tion of hyperelastic models: a feasibil-ity study
Journal of Rubber Research **24** 447—460
 (2021). [https://doi.org/10.1007/](https://doi.org/10.1007/s42464-021-00113-8)
[s42464-021-00113-8](https://doi.org/10.1007/s42464-021-00113-8)
- [35] Pliskin, I., Tokita, N.: Bound Rubber in Elas-
 tomers: Analysis of Elastomer-filler Interac-
 tion and its Effect on Viscosity and Modulus
 of Composite Systems. *Journal of Applied*
Polymer Science **16**, 473–492 (1972). [https://](https://doi.org/10.1002/app.1972.070160217)
doi.org/10.1002/app.1972.070160217

- 1072 the Volume Constraint in Finite Deformation
1073 Elasto-plasticity. *Computer Methods in Applied Mechanics and Engineering*
1074 **51**, 177–208 (1985). [https://doi.org/10.1016/](https://doi.org/10.1016/0045-7825(85)90033-7)
1075 [0045-7825\(85\)90033-7](https://doi.org/10.1016/0045-7825(85)90033-7)
1076
- 1077 [52] Yeoh, O.H.: Some Forms of the Strain Energy
1078 Function for Rubber. *Rubber Chemistry and Technology* **66**(5), 754–771 (1993). [https://](https://doi.org/10.5254/1.3538343)
1079 doi.org/10.5254/1.3538343
1080
- 1081 [53] Morris, M.D.: Factorial Sampling Plans
1082 fo Preliminary Computational Experiments.
1083 *Technometrics* **33**(2), 161–174 (1991).
1084 [https://](https://doi.org/10.1080/00401706.1991.10484804)
1085 doi.org/10.1080/00401706.1991.10484804
1086
- 1087 [54] Iooss, B., Lemaitre, P.: In: Dellino, G., Meloni, C. (eds.) *A Review on Global Sensitivity Analysis Methods*, pp. 101–122. Springer, Boston, MA (2015). [https://doi.org/10.1007/](https://doi.org/10.1007/978-1-4899-7547-8_5)
1088 [978-1-4899-7547-8_5](https://doi.org/10.1007/978-1-4899-7547-8_5)
1089
- 1090 [55] Drucker, D.C.: A Definition of Stable Inelastic Material. *Journal of Applied Mechanics*
1091 **26**, 101–195 (1959). [https://doi.org/10.1115/](https://doi.org/10.1115/1.4011929)
1092 [1.4011929](https://doi.org/10.1115/1.4011929)
1093
- 1094 [56] Inc., A.: *Canonsburg, ANSYS Theory Manual*, (2000)
1095
- 1096 [57] Reynolds, C.W.: Flocks, Herds and Schools: A Distributed Behavioral Model. In: *Proceedings of the 14th Annual Conference on Computer Graphics and Interactive Techniques*, pp. 25–34. Association for Computing Machinery, New York, NY, USA (1987). <https://doi.org/10.1145/280811.281008>
1097
1098
1099
1100
1101
1102
1103
1104
1105
1106
1107
1108
1109
1110
1111
1112
1113
1114
1115
1116
1117
1118
1119
1120
1121
1122
- [58] Brin, S., Page, L.: The Anatomy of a Large-scale Hypertextual Web Search Engine. *Computer Networks and ISDN Systems* **30**(1), 107–117 (1998). [https://doi.org/10.1016/](https://doi.org/10.1016/S0169-7552(98)00110-X)
[S0169-7552\(98\)00110-X](https://doi.org/10.1016/S0169-7552(98)00110-X). *Proceedings of the Seventh International World Wide Web Conference*
- [59] Langville, A.N., Meyer, C.D.: Deeper Inside PageRank. *Internet Mathematics* **1**(3), 335–380 (2004). [https://](https://doi.org/10.1080/15427951.2004.10129091)
doi.org/10.1080/15427951.2004.10129091
- [60] Newton, P.K., Mason, J., Bethel, K., Bazhenova, L.A., Nieva, J., Kuhn, P.: A Stochastic Markov chain Model to Describe Lung Cancer Growth and Metastasis. *PloS one* **7**(4), 34637 (2012). [https://doi.org/10.1371/](https://doi.org/10.1371/journal.pone.0034637)
[journal.pone.0034637](https://doi.org/10.1371/journal.pone.0034637)
- [61] Sutton, M.A., Orteu, J.J., Schreier, H.: *Image Correlation for Shape, Motion and Deformation Measurements: Basic Concepts, Theory and Applications*. Springer (2009)
- [62] Vacher, P., Dumoulin, S., Morestin, F., Mguil-Touchal, S.: Bidimensional Strain Measurement using Digital Images. *Proceedings of the Institution of Mechanical Engineers. Part C: Journal of Mechanical Engineering Science* **213** (1999). [https://doi.org/](https://doi.org/10.1243/0954406991522428)
[10.1243/0954406991522428](https://doi.org/10.1243/0954406991522428)
- [63] Jones, E.M., Iadicola, M.A., et al.: *A Good Practices Guide for Digital Image Correlation*. International Digital Image Correlation Society (2018)